Hindawi
Journal of Chemistry
Volume 2023, Article ID 9893824, 1 page
https://doi.org/10.1155/2023/9893824

*Retraction*

# Retracted: Application of Visual Communication Combined with Electrochemistry in Ceramic Carving Product Design

**Journal of Chemistry**

Received 15 August 2023; Accepted 15 August 2023; Published 16 August 2023

Copyright © 2023 Journal of Chemistry. This is an open access article distributed under the Creative Commons Attribution License, which permits unrestricted use, distribution, and reproduction in any medium, provided the original work is properly cited.

This article has been retracted by Hindawi following an investigation undertaken by the publisher [1]. This investigation has uncovered evidence of one or more of the following indicators of systematic manipulation of the publication process:

(1) Discrepancies in scope
(2) Discrepancies in the description of the research reported
(3) Discrepancies between the availability of data and the research described
(4) Inappropriate citations
(5) Incoherent, meaningless and/or irrelevant content included in the article
(6) Peer-review manipulation

The presence of these indicators undermines our confidence in the integrity of the article's content and we cannot, therefore, vouch for its reliability. Please note that this notice is intended solely to alert readers that the content of this article is unreliable. We have not investigated whether authors were aware of or involved in the systematic manipulation of the publication process.

Wiley and Hindawi regrets that the usual quality checks did not identify these issues before publication and have since put additional measures in place to safeguard research integrity.

We wish to credit our own Research Integrity and Research Publishing teams and anonymous and named external researchers and research integrity experts for contributing to this investigation.

The corresponding author, as the representative of all authors, has been given the opportunity to register their agreement or disagreement to this retraction. We have kept a record of any response received.

## References

[1] J. Geng, "Application of Visual Communication Combined with Electrochemistry in Ceramic Carving Product Design," *Journal of Chemistry*, vol. 2022, Article ID 5768966, 7 pages, 2022.

Hindawi
Journal of Chemistry
Volume 2022, Article ID 5768966, 7 pages
https://doi.org/10.1155/2022/5768966

RETRACTED

*Research Article*

# Application of Visual Communication Combined with Electrochemistry in Ceramic Carving Product Design

**Jian Geng**

*Xijing University, Xi'an, Shaanxi 710123, China*

Correspondence should be addressed to Jian Geng; 202018000893@hceb.edu.cn

Received 10 April 2022; Revised 4 May 2022; Accepted 9 May 2022; Published 14 June 2022

Academic Editor: Ajay Rakkesh R

Copyright © 2022 Jian Geng. This is an open access article distributed under the Creative Commons Attribution License, which permits unrestricted use, distribution, and reproduction in any medium, provided the original work is properly cited.

In order to improve the design of ceramic carving products, the author proposes a visual communication, combined with electrochemistry, laser engraving technology, using superpixel imaging technology, carry out laser engraving ceramic reticulation imaging processing, build a binary laser engraving image model, using image edge feature matching method, carry out the edge contour feature detection of the laser engraved ceramic reticulated image, and extract the local information feature quantity of the laser engraved ceramic mesh image. The fuzzy adaptive segmentation method is used for the extracted features and to perform grid area segmentation. The experimental results show that the greater the laser output power, the deeper the engraving depth. As the laser output power increases, the depth of the hole formed by a single pulse laser is enlarged, the etched area formed by the dense hole group also deepens. However, the experiment found that after the laser power is increased to a certain value (17 A), the temperature of the light spot rises sharply, reach the melting point of ceramics, and produce slag that is not easy to remove on the engraved surface, decrease the effective engraving depth. It proves that visual communication, combined with electrochemistry, can effectively realize the design of ceramic carving products.

## 1. Introduction

Visual communication design is in the continuous development of new media technology, ushered in its own important period of reform. Today's visual communication design has formed a book including book-binding design, printing technology, publicity display, public environment design, digital art design, and comprehensive artistic expression system such as digital photography and videography. This is traditional graphic design, retaining the unique advantages of one's own excellent traditions, and the continuous development of new media technology, the result of mutual learning and fusion [1]. As shown in Figure 1, specifically, in the visual communication design of new media technology, the diversified applications are mainly reflected in.

First, the design tool changes. Traditional visual communication design is mainly drawn by hand. In the design process, paper becomes the main design tool, and in book binding design, painting design, logo design, text design, and commercial promotion design are the main design content. Also, with the development of digital technology, the visual communication design has changed in the design tools; with the continuous development of digital technology and related software technology, the traditional paper hand-drawn design method, replaced by computer software, specifically, contains digital drawing tools, digital photography image shooting tools, etc. [2]. For example, the well-known Dreamweaver, Photoshop, AutoCAD, etc. are all specific application software for digital drawing in web page drawing, image processing, and industrial drawing. Paperless design has changed the design stage in the past, which required a lot of paper to draw in inefficient working conditions; at the same time, the continuous development of digital photography and camera technology also makes visual communication design gradually moved towards the direction of multidimensional dynamic visual communication [3].

Second, the status of the media has changed. We all know the traditional visual communication design and the degree of dependence on paper makes its dissemination

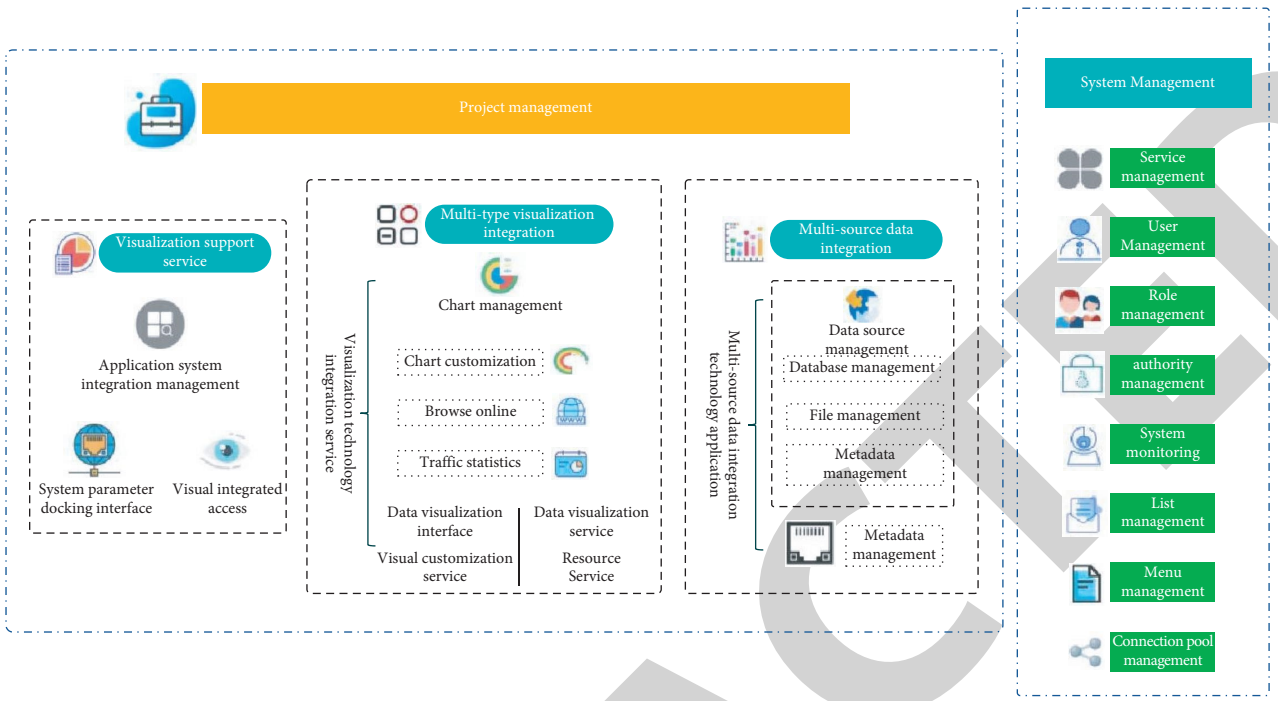


Figure 1: Visual communication combined with electrochemistry.

carrier still stay in the era of printing technology. As a result, printing technology has become an important factor in the development of traditional visual communication design. Product packaging design is also in the innovation of printing technology, an important topic that has been paid attention to by the industry. With the popularity of the Internet and the rise of digital media, in the technological revolution of digital technology, visual communication design under the impact of digital control technology and a variety of digital communication media have also emerged at the historic moment [4]. The new media can realize the visual transmission effect of pictures, texts, characters, and sounds; at the same time, the characteristics and advantages of the times displayed by the new media also makes digital technology in the field of visual communication design much favored; at the same time, the continuous development of digital control technology has also had a wide-ranging impact in the printing industry. Therefore, under the background of the sudden emergence of new media and the integration of new and old media, the status of the media of visual communication design has quietly changed [5].

## 2. Literature Review

Zheng, with the help of visual symbols, transferred and used information resources. In this process, the use of technology plays an important role. With the continuous improvement of the level of social science and technology, multimedia technology has been well developed and applied to visual communication design. With the effective combination of the two, the quality and efficiency of visual communication design have been improved to a certain extent [6]. Liu et al. proposed that multimedia technology has a visual guidance function, can promote the memory of the audience, and facilitate the refinement and screening of useful information by the audience. Multimedia technology not only to a certain extent promote the prosperity and development of art but also provides a platform for the inheritance of traditional art [7]. Yang et al. stated that in the context of the development of the era of integrated media, multimedia technology is widely used in visual communication design. It not only improves the quality of visual communication design but also promotes the innovative development of visual communication design. Applying multimedia technology to visual communication design [8], Yan combined Sketchup, AutoCAD, and other software for laser engraving, performed 3D modeling of ceramic reticulated defects, used association matching and template detection methods, and carried out the detection of ceramic reticulation defects in laser engraving [9]. Corrales-Garcia et al. proposed a laser engraving based on differential scanning of key points, ceramic reticulation defect detection, and positioning method, used infrared feature scanning and holographic projection technology, performed image segmentation and scanning of ceramic anilox defects in laser engraving, improved the defect detection ability. This method is not good for the detection performance of small defects [10]. Bera et al. proposed a differential scan based on moving frames, adaptive compensation laser engraving, and ceramic reticulation defect detection method. This method uses block technology, in order to achieve the reconstruction of the three-dimensional contour and the matching of the image template; however, during the detection process of this method, there is a problem of weak adaptive repair ability [2]. Choi et al. used lasers to perform complex forming and processing of ceramics, and it has always been a difficult point in laser processing [11]. Liao et al., using laser technology and

RETRACTED

processing microtexture on the surface of aluminum substrate, successfully manufactured a low-adhesion double sparse surface, with excellent performance in anti-icing and self-cleaning [12]. Bourdonnec et al., using lasers, on the surface of polydimethylsiloxane, successfully prepared a superhydrophobic surface imitating reed leaves [13]. Ladeesh and Manu used laser engraving, on the surface of composite insulator silicone rubber, processing various textures, and the effect of texture shape, spacing and depth on hydrophobicity is obtained [14].

Based on the current research, we propose a laser engraving based on Harris corner detection and automatic detection method of ceramic reticulation defects, using superpixel imaging technology, and carry out laser engraving ceramic reticulation imaging processing and build a binary laser engraving image model, by extracting the feature vector, combined with fuzzy adaptive segmentation method. The segmentation of the grid area is realized.

## 3. Image Collection and Feature Preprocessing of Ceramic Reticulated Defects in Laser Engraving

*3.1. Laser-Engraved Ceramic Reticulation Image Collection.* In order to realize the detection of ceramic anilox defects in laser engraving, combining image restoration and 3D multimedia reconstruction methods, and realize laser engraving defect detection and positioning, the first step is to use the ray-casting image feature scanning method, construct 3D multimedia contours of defect images, realize the image collection of ceramic reticulated defects in laser engraving, use the image space scanning method of ceramic reticulated defects in laser engraving (common ones such as cell projection and splatting), use the feature scanning method to extract brightness features and texture features according to the feature extraction results, carry out automatic detection of defective parts based on the difference of the brightness feature to the moving frame of the superpixel, and perform template registration, thereby improving the detection ability of ceramic reticulation defects in laser engraving [15].

Assuming that the local noise reduction domain near each point in the image is $\Omega$, engraving ceramic mesh image $I(x, y)$ on grayscale laser, use dividing line $C$ to divide into two areas $R_1$ and $R_2$. The total number of blocks on both sides of the target boundary of the image is $K$. Using the GMM Gaussian Mixture Model, describe the marking process of laser-engraved ceramic mesh image pixels. The imaging output of the laser-engraved ceramic mesh image is

$$\frac{\partial u(x, y; t)}{\partial t} = \frac{\partial^2 u(x, y; t)}{\partial \xi^2} + c^2 \frac{\partial^2 u(x, y; t)}{\partial \eta^2}. \tag{1}$$

Relying on the neighborhood segmentation curve for pixel feature matching, the texture subspace of the superpixel laser-engraved ceramic mesh image is expressed as

$$\begin{bmatrix} x \\ y \end{bmatrix} = \begin{bmatrix} \cos\theta & -\sin\theta \\ \sin\theta & \cos\theta \end{bmatrix} \begin{bmatrix} \xi \\ \eta \end{bmatrix}. \tag{2}$$

In the above formula,

$$\theta = \arctan\begin{pmatrix} \dfrac{\partial u}{\partial y} \\ \dfrac{\partial u}{\partial x} \end{pmatrix}. \tag{3}$$

By presetting the correlation $K$, in the laser engraving, the sparse linear equations for matching the image template of the ceramic anilox defect image are as follows:

$$g(x, y) = h(x, y) \times f(x, y) + \eta(x, y). \tag{4}$$

In formula (4), $h(x, y)$represents the parallax function of the ceramic reticulated defect, and $\times$ represents convolution. Using the edge detection algorithm to realize image information fusion, we get

$$c = \sqrt{\exp\left[-\frac{1}{K}|\nabla u(x, y; t)|\right]}. \tag{5}$$

In order to realize the region merging after superpixel segmentation, the laser-engraved ceramic mesh image area is divided into various sub-blocks. The scale of the sub-block is $M$, and M-1 iterations are performed. The iterative formula for saliency superpixel discrimination is as follows:

$$d_{i+1} = 2F\left(x_{i+1} + \frac{1}{2}, y_i + 2\right) = \begin{cases} 2\left[\Delta x(y_i + 2) - \Delta y\left(x_{i,r} + \dfrac{1}{2} - \Delta x B\right)\right], & d_i \le 0, \\ 2\left[\Delta x(y_i + 2) - \Delta y\left(x_{i,r} + \dfrac{1}{2} - \Delta x B\right)\right], & d_i > 0. \end{cases} \tag{6}$$

Calculated in the laser engraving under texture mapping transformation and chromatic aberration, the difference pixel value of the image feature extraction of ceramic anilox defect was obtained and then get the laser engraving. The estimated value of the edge pixel of the ceramic reticulation defect is

$$\widehat{f}(x, y) = \beta F(x, y) + (1 - \beta) m_l + \delta_l^2. \tag{7}$$

The strong texture concentration of laser-engraved anilox defect image was calculated. $(x, y)$ represents the scanning point, $F(x, y)$ represents the pixel value, $\delta_l^2$ represents the local variance, and $m_l$ represents the weak texture set of the defect location [16].

*3.2. Image Edge Contour Feature Detection.* Based on template matching and image block processing, through the realization of image training samples, the main feature vector space is constructed. In the process of image laser engraving and image reconstruction processing of ceramic reticulation defects, establish the local gradient energy distribution function of ceramic reticulated defects as follows:

RETRACTED

$$x_{i,d}^{k+1} = \begin{cases} 1, & \rho_{i,d}^{k+1} \le \mathrm{sig}\left(v_{i,d}^{k+1}\right), \\ 0, & \rho_{i,d}^{k+1} \le \mathrm{sig}\left(v_{i,d}^{k+1}\right). \end{cases} \tag{8}$$

In the above formula, $\rho_{i,d}^{k+1} \in [0, 1]$ is a geometric feature, $\mathrm{sig}(\cdot)$ is the Sig-moid function. Use metrics to control superpixels denoted as $C = \{(x, y) \in \Omega: \phi(x, y) = 0\}$ and get the brightness characteristics of the image:

$$\mathrm{sig}\left(v_{i,d}^{k+1}\right) = \frac{1}{1 + e^{-v_{i,d}^{k+1}}}. \tag{9}$$

Use pixel $i$ as the base point to achieve image segmentation. The scope is carried out in the affine invariant area of the image. Suppose the geometric feature vectors $e_1, e_2, \ldots, e_l$, of the first $l$ laser-engraved ceramic mesh image. In the overlapping area, the iterative equation of the image reconstruction error in the holographic projection area is as follows:

$$\begin{aligned} v_{i,d}^{k+1} = {} & w \cdot v_{i,d}^{k} + c_1 \cdot \mathrm{rand}() \cdot \left(c_3 \cdot \mathrm{rand}() \cdot p\mathrm{best}_{i,d}^{k} - x_{i,d}^{k}\right) \\ & + c_2 \cdot \mathrm{rand}() \cdot \left(c_2 \cdot \mathrm{rand}() \cdot g\mathrm{best}_{d}^{k} - x_{i,d}^{k}\right). \end{aligned} \tag{10}$$

Among them, $c_3 \cdot \mathrm{rand}()$ and $c_4 \cdot \mathrm{rand}()$ are called the Harris corners of the reticulated image, and the expression is

$$\begin{aligned} c_3 \cdot \mathrm{rand}() &= \begin{cases} 1, & e_p > e_{0p}, \\ c_3 \cdot \mathrm{rand}(), & e_p \le e_{0p}, \end{cases} \\ c_4 \cdot \mathrm{rand}() &= \begin{cases} 1, & e_g > e_{0g}, \\ c_4 \cdot \mathrm{rand}(), & e_g \le e_{0g}. \end{cases} \end{aligned} \tag{11}$$

$x_{ij} \in [x_{\min}, x_{\max}]$ and $\overline{X}_i = (\overline{x}_{i1}, \overline{x}_{i2}, \ldots, \overline{x}_{ij}, \overline{x}_{i\,D})$ are called the difference feature of image edge contour feature detection [17]. For the gray sample set $(x_i, y_i)$ of the image of the ceramic anilox defect in laser engraving, use $x_i$ for input and $y_i$ for corresponding output. In the laser engraving, the characteristic distribution function of ceramic reticulated defects is

$$f(x) = w^T \phi(x) + b. \tag{12}$$

In the formula, $W$ is the image edge contour feature detection and $b$ is the offset. The distance between each pixel point and cluster center was calculated, and the partial detection information of ceramic mesh defect image in laser engraving was obtained according to the similarity of different features [18]. Thus, the image constraint control 3D multimedia reconstruction model is obtained:

$$\begin{aligned} & \min_{w,b,e} J(w, e) = \frac{1}{2} W^T W + \frac{C}{2} \sum_{i=1}^{n} e_i^2, \\ & \text{s.t. } y_i = w^T \phi(x) + b + e_i, \\ & i = 1, 2, \ldots, l. \end{aligned} \tag{13}$$

In the formula, $C$ is the penalty parameter and $e_i$ is the defect detection error. According to the above analysis, the template matching and 3D multimedia edge contour segmentation are carried out by using the block technique, and the feature location of ceramic reticular defect in laser engraving is carried out according to the regional sample attributes of 3D multimedia contour [19].

## 4. Experimental Results and Analysis

Under the condition that the laser scanning speed is 25 mm/s and the repetition frequency is 2 kHz, the relationship curve of the influence of laser power (characterized by current, the same below) on the depth of engraving, is shown in Figure 2. The results show, the greater the laser output power, the deeper the engraving depth. With the increase of laser output power, the depth of the hole formed by a single pulse laser increases and the etched area formed by dense hole groups also deepens. However, the experiment found that after the laser power is increased to a certain value (17 A), the temperature of the light spot rises sharply, when the melting point of ceramics is reached, and slag that is not easy to be removed is generated on the engraving surface, which reduces the effective engraving depth [20].

As shown in Figure 3, under the conditions of a laser power of 12 A and a repetition frequency of 2 kHz, the law of engraving depth changes with the laser scanning speed. As can be seen, if the laser scanning speed is too large or too small, the engraving depth will be reduced; only when the scanning speed is moderate (15 mn/s at this time), the engraving depth increases significantly. If the laser repetition frequency remains the same, increasing the scanning speed will cause the overlap of the laser spot to decrease, and the engraving depth will decrease significantly [21]. Too small scan speed will cause unit time, the laser energy received by the engraving surface increases, and slag is produced, which also reduces the depth of engraving [22]. Under the condition that the laser scanning speed is 25 m-n/s and the laser power is 12 A, engraving depth and the relationship with the change of laser pulse repetition frequency is shown in Figure 4. The engraving depth increases with the increase of the repetition frequency, after reaching a certain value (2.0 kHz), and the engraving depth began to show a downward trend. Increase in repetition frequency means that the energy received by the carving area at the same time increases and the number of interactions between the laser and the material increases, resulting in partial melting of the ceramic, and slag is generated on the engraving surface, which reduces the effective engraving depth.

On the original ceramic surface and the surface of each texture sample with the best hydrophobic performance, drop 40 $\mu L$ droplets, affix the label and serial number for future use. The TEMI880 series humidity temperature programmable controller was used for temperature setting at −10°C, and the humidity is 80%. When the temperature in the instrument stabilizes at (−10 ± 0.5)°C, put the samples to be tested in the order of the labels, and start the timing. Observe through the window until the droplet becomes completely white. Take it out and end the timing [23]. When the time is 80 s, the water droplets on the surface of the original ceramics is observed, and ice crystals have begun to appear; however, the water droplets on the surface of the three

RETRACTED

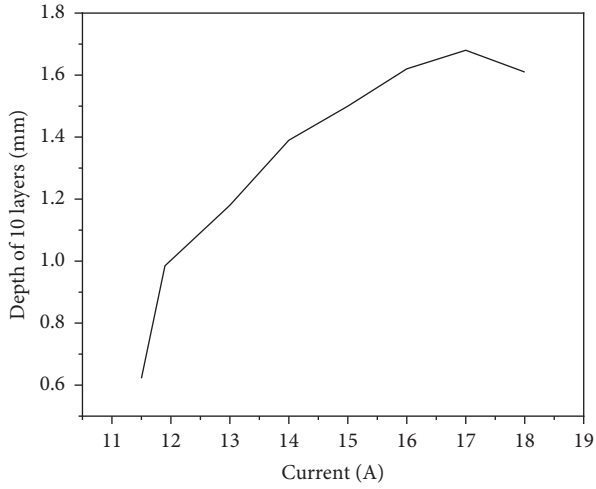


Figure 2: The relationship between laser power and engraving depth.

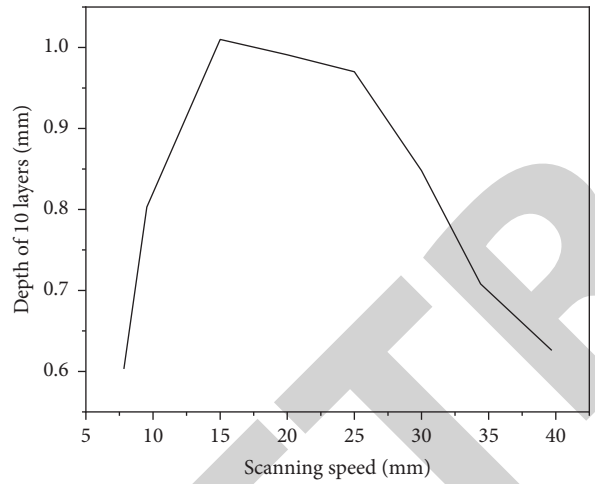


Figure 3: The relationship between scanning speed and engraving depth.

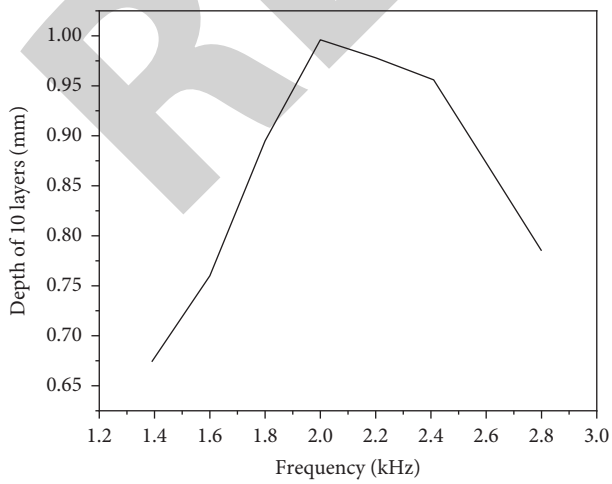


Figure 4: The relationship between laser pulse frequency and engraving depth.

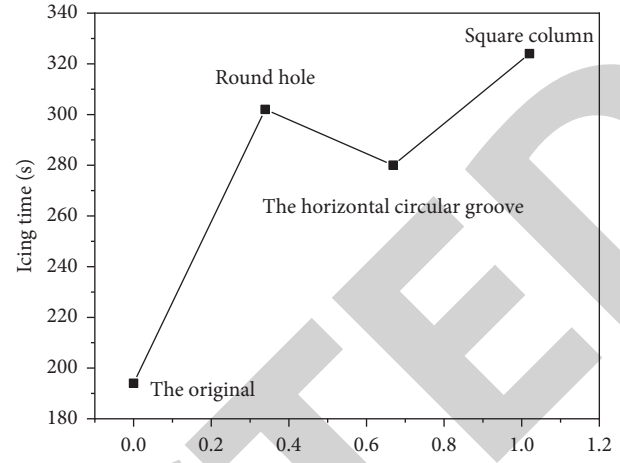


Figure 5: Comparison of average freezing time on textured surface.

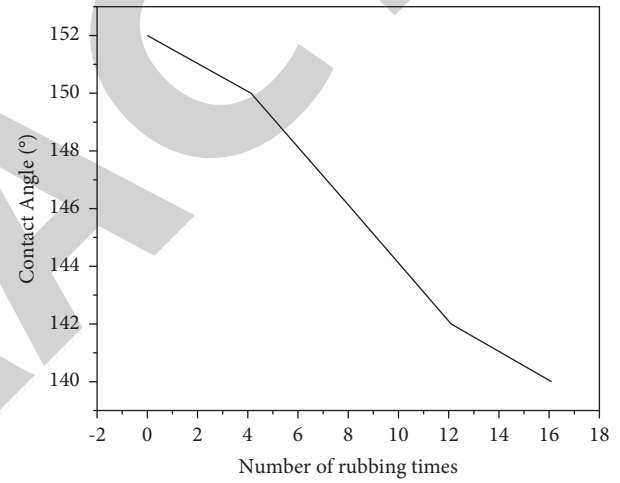


Figure 6: The contact angle of the surface of the transverse groove changes with the number of friction.

textures remained unchanged. When the time is 220 s, the water droplets on the textured surface gradually begin to become ice crystals. When the time is 280 s, the water droplets on the surface of the transverse groove texture are completely frozen, and the test results are shown in Figure 5. The results showed that, after the texturing treatment, the anti-icing performance of the sample is obviously improved with delayed freezing time. This is due to the small contact angle of water droplets on the original ceramic surface. The contact area between the two is larger, so the heat transfer speed is faster. The contact angles of water droplets on the textured ceramic surface are all greater than 150°. Reduce the contact area between water droplets and the ceramic surface, delay the heat transfer, and then delay the freezing time.

In order to study the superhydrophobicity of the prepared surface and durability of anti-icing properties, conduct abrasion resistance tests on samples of various types of optimal textures. The author uses an accelerated test method, in order to make the surface friction greater. A weight of 200 g was used to pressurize the sample, and move back and forth on the sandpaper of model number 3000. After moving

RETRACTED

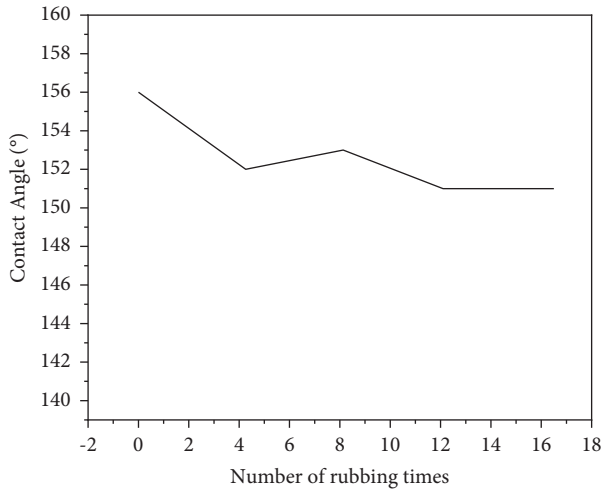


Figure 7: The contact angle of the surface of the square column varies with the number of frictions.

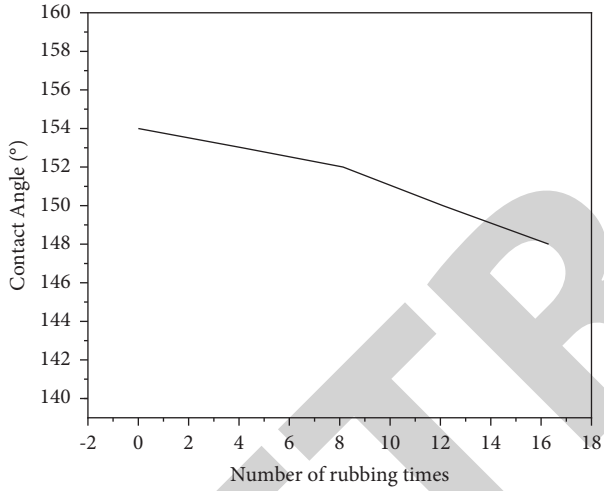


Figure 8: The contact angle of the surface of the round hole changes with the number of friction.

15 cm to the right, returning to the original path is a friction. After each rubbing, clean the surface, the contact angle of the test surface [24]. The contact angle and 3-dimensional multimedia topography after 10 times of friction are shown in Figures 6, 7, and 8. The contact angle changes after the friction times are 0, 4, 8, 12, and 16, respectively.

The test results show that as the number of frictions increases, the contact angle of each texture surface decreased slightly but not much. The square column texture surface is within the friction times of the test, still maintaining a superhydrophobic state; however, when the surface of the transverse groove texture is rubbed more than 12 times, the texture loses its hydrophobicity, and when the round hole texture surface is rubbed more than 16 times, superhydrophobicity is lost.

## 5. Conclusion

The thickness of single-layer slices must be ensured to be equal to the actual depth of each layer engraved by the laser. It is the key to the process of laser 3D multimedia engraving. For a selected engraving material, as long as the process parameters are properly selected, under the premise of ensuring the quality of engraving, obtain a precise single-layer engraving depth. Explore the laser engraving depth and the law of changes with process parameters, and establish a mathematical model of engraving, which helps in the experiment, quickly obtain the parameter data that meets the needs of the process, and provide data basis for laser 3D multimedia engraving. The successful engraving of three-dimensional multimedia five-pointed star graphics not only shows that the principle of layered forming can be applied to the field of laser engraving but also provides an industrial verification for the laser 3D multimedia engraving system.

## Data Availability

The data used to support the findings of this study are available from the corresponding author upon request.

## Conflicts of Interest

The author declares that there are no conflicts of interest.

## References

[1] Y. C. Wang, Y. Ma, W. Z. Yu, Y. F. Li, and Y. H. Liu, "Application of the computer assisted virtual reduction combined with 3d printing technique in acetabular fractures," *China Journal of Orthopaedics and Traumatology*, vol. 30, no. 7, pp. 627–632, 2017.

[2] S. Bera, S. N. Sur, and R. Bera, "Multimedia communication using dvb technology over open range," *Procedia Computer Science*, vol. 70, pp. 282–288, 2015.

[3] F. He, "Industrial product graphic design based on visual communication concept," *Acta Technica CSAV (Ceskoslovensk Akademie Ved)*, vol. 62, no. 1, pp. 269–278, 2017.

[4] X. Xi, "Design and manufacture of pe multimedia network courseware under the web environment," *Agro Food Industry Hi-Tech*, vol. 28, no. 1, pp. 1621–1626, 2017.

[5] Q. Zhou, X. Li, K. He, Y. Sheng, and N. Zhang, "Application of intraoperative mri combined with neuronavigation in microsurgical resection for insular glioma," *Journal of Central South University. Medical Sciences*, vol. 43, no. 4, pp. 383–387, 2018.

[6] D. Zheng, "Research on application of computer 3d modeling technology in ceramic tea set design," *Journal of Physics: Conference Series*, vol. 1961, no. 1, Article ID 012058, 2021.

[7] D. Liu, Z. Wu, X. Lin, and R. Ji, "Towards perceptual video cropping with curve fitting," *Multimedia Tools and Applications*, vol. 75, no. 20, pp. 12465–12475, 2016.

[8] Q. Yang, H. Wang, M. Dohler, Y. Wen, and G. Xue, "Guest editorial multimedia communication in the internet of things," *IEEE Internet of Things Journal*, vol. 4, no. 2, pp. 484–486, 2017.

[9] R. Yan, "The rise of multimedia for online communication startups," *IEEE Multimedia*, vol. 22, no. 4, pp. 100–104, 2015.

[10] A. Corrales-Garcia, R. Rodriguez-Sanchez, J. L. Martínez, G. Fernandez-Escribano, and F. J. Quiles, "Multimedia communications using a fast and flexible dvc to h.264/avc/svc transcoder," *Journal of Signal Processing Systems*, vol. 79, no. 3, pp. 211–232, 2015.

[11] J.-H. Choi, U. S Kim, and W.-S. Cho, "Study on ceramic pattern carving by using laser—focused on glaze's melting

RETRACTED

effect," *Journal of Digital Design*, vol. 15, no. 1, pp. 703–710, 2015.

[12] Z. Liao, T. Zhang, M. Gall et al., "Lateral damage in graphene carved by high energy focused gallium ion beams," *Applied Physics Letters*, vol. 107, no. 1, Article ID 013108, 2015.

[13] F. Bourdonnec, A. D'Anna, G. Poupeau et al., "Obsidians artefacts from Renaghju (Corsica island) and the early Neolithic circulation of obsidian in the western Mediterranean," *Archaeological and Anthropological Sciences*, vol. 7, no. 4, pp. 463-464, 2015.

[14] V. G. Ladeesh and R. Manu, "Machining of fluidic channels on borosilicate glass using grinding-aided electrochemical discharge engraving (g-ecde) and process optimization," *Journal of the Brazilian Society of Mechanical Sciences and Engineering*, vol. 40, no. 6, p. 299, 2018.

[15] C. C. Ho and D. S. Wu, "Characteristics of the arcing plasma formation effect in spark-assisted chemical engraving of glass, based on machine vision," *Materials*, vol. 11, no. 4, p. 470, 2018.

[16] M. K. Mohammed, A. Al-Ahmari, and U. Umer, "Multi-objective optimization of nd:yag direct laser writing of microchannels for microfluidic applications," *International Journal of Advanced Manufacturing Technology*, vol. 81, no. 5–8, pp. 1363–1377, 2015.

[17] J. Y. Hong, D. L. Way, Z. C. Shih, W. K. Tai, and C. C. Chang, "Inner engraving for the creation of a balanced lego sculpture," *The Visual Computer*, vol. 32, no. 5, pp. 569–578, 2016.

[18] A. Vankevich and I. Kalinouskaya, "Ensuring sustainable growth based on the artificial intelligence analysis and forecast of in-demand skills," *E3S Web of Conferences*, vol. 208, no. 79, Article ID 03060, 2020.

[19] M. A. Kipriyanova and S. N. Smolnikov, "Sociological analysis of the problem of ecological justice," *Historical and Social-Educational Ideas*, vol. 10, pp. 117–126, 2019.

[20] R. Kyere-Boateng and M. V. Marek, "Analysis of the social-ecological causes of deforestation and forest degradation in Ghana: application of the dpsir framework," *Forests*, vol. 12, no. 4, p. 409, 2021.

[21] R. Huang, P. Yan, and X. Yang, "Knowledge map visualization of technology hotspots and development trends in China's textile manufacturing industry," *IET Collaborative Intelligent Manufacturing*, vol. 3, no. 3, pp. 243–251, 2021.

[22] X. Liu, J. Liu, J. Chen, and F. Zhong, "Degradation of benzene, toluene, and xylene with high gaseous hourly space velocity by double dielectric barrier discharge combined with $Mn_3O_4$/activated carbon fibers," *Journal of Physics D: Applied Physics*, vol. 55, no. 12, Article ID 125206, 2022.

[23] J. Jayakumar, B. Nagaraj, and P. Ajay, "Conceptual implementation of artificial intelligent based E-mobility controller in smart city environment," *Wireless Communications and Mobile Computing*, vol. 2021, Article ID 5325116, 8 pages, 2021.

[24] G. Dhiman, V. Vinoth Kumar, A. Kaur, and A. Sharma, "Don: deep learning and optimization-based framework for detection of novel coronavirus disease using x-ray images," *Interdisciplinary Sciences: Computational Life Sciences*, vol. 13, no. 2, pp. 260–272, 2021.

RETRACTED